Journal of Thermal Analysis, Vol. 48 (1997) 1379-1384

STUDIES ON THE NON-ISOTHERMAL KINETICS OF THERMAL DECOMPOSITION OF THE MIXED LIGAND COMPLEX – $[Fe_2O(OC_6H_4CH{=}NC_6H_4O)_2(C_5H_5N)_4]\cdot 2H_2O$

Qing-Ping Hu, Xue-Gui Cui and Zhao-He Yang***

Department of Chemistry, Shandong University, Jinan, 250100
**Institute of Crys. Mat., Shandong University, Jinan, 250100, P.R.China

(Received December 8, 1995; in revised form August 13, 1996)

Abstract

The thermal decomposition of the mixed-ligand complex of iron(III) with 2-[(*o*-hydroxy benzylidene)amino] phenol and pyridine-$[Fe_2O(OC_6H_4CH{=}NC_6H_4O)_2(C_5H_5N)_4]\cdot 2H_2O$ and its non-isothermal kinetics were studied by TG and DTG techniques. The non-isothermal kinetic data were analyzed and the kinetic parameters for the first and second steps of the thermal decomposition were evaluated by two different methods, the Achar and Coats-Redfern methods. Steps 1 and 2 are both second-order chemical reactions. Their kinetic equations can be expressed as:

$$d\alpha/dt = Ae^{-E/RT}(1-\alpha)^2$$

Keywords: coupled technique, iron(III) compound, non-isothermal, Schiff base complex

Introduction

Complexes of transition metals with some Schiff bases are of increasing interest because they can be used as anticancer medicine, preservative and antibacterial agent [1–3]. In particular, the biochemical behaviour and function of iron(III) has a direct bearing on human health. In order to study the relationship between the structure and their syntheses, properties, applications, a series of Schiff base complexes have been synthesized [4–5]. The present work reports the studies on the kinetics and mechanism of the non-isothermal thermal decomposition of the title complex by TG and DTG.

Experimental

The title complex was synthesized and its structure was determined by means of single crystal X-ray diffraction method according to procedures reported in a previous work [6].

* Author to whom all correspondence should be addressed.

0368–4466/97/ $ 5.00

John Wiley & Sons Limited
Chichester

TG and DTG curves were recorded simultaneously by a TGS-2 type thermal analyser (Perkin-Elmer USA). The heating rate was 10°C min^{-1} and the flow rate of nitrogen was 40 cm^3 min^{-1}.

Results and discussion

TG and DTG curves of the complex are shown in Fig. 1, which shows that the complex decomposes in three stages:

$$[Fe_2O(OC_6H_4CH{=}NC_6H_4O)_2(C_5H_5N)_4]{\cdot}2H_2O \xrightarrow[\text{exp. mass loss, 37.39\%; calcd., 38.91\%}]{50\text{–}270^\circ C}$$

$$Fe_2O(OC_6H_4CH{=}NC_6H_4O)_2 \xrightarrow[\text{exp. mass loss, 10.78\%; calcd., 10.25\%}]{270\text{–}390^\circ C}$$

$$Fe_2O(OC_6H_4CH{=}NC_6H_4O)(OC_6H_4CH{=}N) \xrightarrow[\text{exp. mass loss, 34.08\%; calcd., 33.18\%}]{390\text{–}530^\circ C}$$

Fe_2O_3 (residual exp. mass 17.72% and calculated 17.56%)

Structure determination [11] showed that each of the iron atoms was coordinated with two nitrogen atoms from two Py molecules respectively, two oxygen and one nitrogen atoms from the other ligand and the oxygen combining with two iron atoms to form an octahedron. The two Py molecules were symmetrical with respect to the plane which consisted of the iron atom, the oxygen atom from the oxygen bridge, the nitrogen and the two oxygen atoms from the other ligand. On the other hand, the bond distances of Fe–O (from the ligand) were found to be 0.197–0.198 nm, the bond distances of Fe–N 0.22–0.23 nm and the bond distances of Fe–O (combining with two iron atoms) 0.17–0.18 nm. Therefore, the dehydration and the loss of four Py molecules take place in the first step. In all of the coordinate bonds, it is

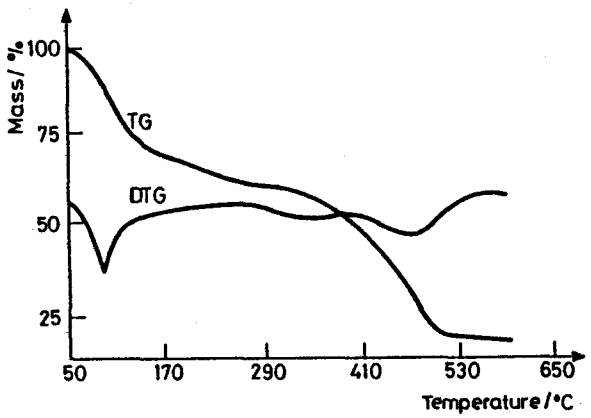

Fig. 1 TG and DTG curves of the complex

the most difficult for the oxygen bridge bond between two iron atoms to be broken, leading to a residual mass corresponding to Fe_2O_3 as confirmed by X-ray diffraction.

The mechanisms of the first and second steps of the thermal decomposition reaction were determined by the Achar method (differential method) and the Coats-Redfern method (integral method) through comparing the kinetic parameters of probable kinetic model functions.

Achar equation [7]:

$$\ln[(d\alpha/dt)f(\alpha)] = \ln A - E/RT \quad (1)$$

Coats-Redfern equation [8]:

$$\ln[(g(\alpha)/T^2] = \ln(AR/\beta E) - E/RT \quad (2)$$

where $f(\alpha)$ and $g(\alpha)$ are differential and integral mechanism functions, respectively, α is the thermal decomposed fraction at temperature T/K, β is the heating rate, E is the derived apparent activation energy, A is the pre-exponential factor and R is the gas constant.

By substituting the non-isothermal kinetic original data α, T and $d\alpha/dt$ for the thermal decompositions of step 1 and step 2 obtained by analyzing the TG and DTG curves (list in Table 1), and the probable mechanism functions $f(\alpha)$ and $g(\alpha)$, given in Table 2, into Eq. (1) and Eq. (2) respectively, the values for the non-isothermal kinetic parameters E, A and correlation coefficient r of the different kinetic model functions were obtained (listed in Tables 3 and 4, respectively) by the linear least-squares method.

Table 1 Non-isothermal kinetic data of the thermal decomposition of the complex

The first-step thermal decomposition				The second-step thermal decomposition			
No.	α_i	T_i/K	$(d\alpha/dt)_i$/min^{-1}	No.	α_i	T_i/K	$(d\alpha/dt)_i$/min^{-1}
1	0.0268	343	0.5993	1	0.1271	593	8.071
2	0.0394	353	1.599	2	0.1865	603	10.47
3	0.1309	363	3.437	3	0.2709	608	11.30
4	0.3046	373	5.436	4	0.3933	613	12.11
5	0.4843	383	3.917	5	0.4564	618	12.51
6	0.5691	393	2.318	6	0.5260	623	11.29
7	0.6329	403	1.959	7	0.6354	633	9.684
8	0.6798	413	1.679	8	0.7495	643	7.263
9	0.7243	423	1.599	9	0.8868	653	5.650
10	0.7951	433	1.439	10	0.9434	658	4.034
11	0.8418	453	1.359				
12	0.9533	483	1.080				
13	0.9928	523	0.6395				

Table 2 Kinetic functions used for the analysis

Mechanism	Integral form, $g(\alpha)$	Differential form, $f(\alpha)$
P1 Power law	$\alpha^{1/4}$	$4\alpha^{3/4}$
	$\alpha^{1/3}$	$3\alpha^{2/3}$
	$\alpha^{1/2}$	$2\alpha^{1/2}$
	α	1
A1.5 Avrami-Erofeev	$[-\ln(1-\alpha)]^{2/3}$	$1.5(1-\alpha)[-\ln(1-\alpha)]^{1/3}$
A2 Avrami-Erofeev	$[-\ln(1-\alpha)]^{1/2}$	$2(1-\alpha)[-\ln(1-\alpha)]^{1/2}$
A3 Avrami-Erofeev	$[-\ln(1-\alpha)]^{1/3}$	$3(1-\alpha)[-\ln(1-\alpha)]^{2/3}$
A4 Avrami-Erofeev	$[-\ln(1-\alpha)]^{1/4}$	$4(1-\alpha)[-\ln(1-\alpha)]^{3/4}$
R2 Contracting surface	$1-(1-\alpha)^{1/2}$	$2(1-\alpha)^{1/2}$
R3 Contracting volume	$1-(1-\alpha)^{1/3}$	$3(1-\alpha)^{2/3}$
D1 1-D diffusion	α^2	$1/2\alpha$
D2 2-D diffusion	$(1-\alpha)\ln(1-\alpha)+\alpha$	$-[\ln(1-\alpha)]^{-1}$
D3 3-D diffusion	$[1-(1-\alpha)^{1/3}]^2$	$1.5[1-(1-\alpha)^{4/3}]^{-1}(1-\alpha)]^{2/3}-1$
D4 Ginstling-Brounshtein	$(1-2\alpha/3)-(1-\alpha)^{2/3}$	$1.5[(1-\alpha)^{-1/3}-1]^{-1}$
F1 First-order	$-\ln(1-\alpha)$	$1-\alpha$
F2 Second-order	$(1-\alpha)^{-1}-1$	$(1-\alpha)^2$

Table 3 Kinetic parameters of the first-step thermal decomposition of the complex obtained by Achar and Coats-Redfern methods

	Achar method			Coats-Redfern method		
Mechanism	E/kJ mol^{-1}	$\ln A/s^{-1}$	r	E/kJ mol^{-1}	$\ln A/s^{-1}$	r
P1	-28.45	-8.55	0.9435	0.16	-6.98	0.0314
	-26.09	-7.64	0.9336	2.52	-3.59	0.3587
	-21.38	-6.00	0.8937	7.23	-1.30	0.6009
	-7.22	-1.60	0.4003	21.39	3.49	0.7502
A1.5	15.12	6.09	0.7136	20.38	3.82	0.8731
A2	8.30	3.85	0.4770	13.56	1.47	0.8436
A3	1.47	1.50	0.0904	6.73	-1.18	0.7533
A4	-1.94	0.24	0.1149	3.32	-2.86	0.5933
R2	10.77	3.70	0.5988	26.50	4.76	0.8208
R3	16.77	5.29	0.7587	28.70	5.18	0.8462
D1	21.08	6.50	0.5364	49.69	11.7	0.7798
D2	33.73	10.1	0.7334	55.46	13.5	0.8302
D3	52.39	14.8	0.8851	64.32	14.8	0.8740
D4	40.39	10.8	0.8057	58.27	12.6	0.8453
F1	28.77	10.4	0.8808	34.03	8.23	0.8958
F2	64.76	22.4	0.9360	57.38	16.5	0.9747

Table 4 Kinetic parameters of the second-step thermal decomposition of the complex obtained by Achar and Coats-Redfern methods

	Achar method			Coats-Redfern method		
Mechanism	E/kJ mol^{-1}	ln$A$/s^{-1}	r	E/kJ mol^{-1}	ln$A$/s^{-1}	r
P1	-111.8	-20.2	0.9824	13.72	-0.72	0.8846
	-103.8	-18.4	0.9764	21.76	1.22	0.9150
	-87.72	-15.0	0.9567	37.85	4.73	0.9353
	-39.47	-5.44	0.7096	86.10	14.4	0.9493
A1.5	38.95	10.4	0.8955	87.51	15.3	0.9877
A2	14.47	5.46	0.6111	63.03	10.3	0.9866
A3	-10.01	0.41	0.4706	38.55	5.17	0.9840
A4	-22.25	-2.21	0.7604	26.31	2.46	0.9806
R2	24.22	6.64	0.7421	108.1	18.4	0.9742
R3	45.45	10.5	0.9221	116.8	19.8	0.9803
D1	57.04	13.0	0.6525	182.6	33.0	0.9548
D2	107.0	22.5	0.8909	208.6	37.7	0.9687
D3	172.6	34.1	0.9736	244.0	43.4	0.9819
D4	130.2	25.5	0.9366	220.1	38.5	0.9739
F1	87.91	20.1	0.9696	136.5	25.0	0.9887
F2	215.3	45.7	0.9620	213.5	40.9	0.9886

The results in Tables 3 and 4 clearly show that the values E and A obtained from the two equations are approximately the same and the linear correlation coefficients are better when the probable mechanism function is logically F2 (in Table 2). We concluded that both steps 1 and 2 are second-order chemical reactions. The mechanism functions for both steps 1 and 2 are:

$$f(\alpha) = (1 - \alpha)^2, \qquad g(\alpha) = (1 - \alpha)^{-1} - 1$$

correspondingly, the non-isothermal kinetic equations are:

$$d\alpha/dt = Ae^{-E/RT}(1 - \alpha)^2 \quad \text{(Second-order chemical reaction)}$$

* * *

The project was supported by the National Laboratory of Crystal Materials, Shandong University Fundation.

References

1 Z. S. Wu, J. Central China Teachers College, 1 (1983) 61.
2 B. Y. Yu and H. W. Zhen, J. Inorg. Chem., 4 (1988) 97.

3 X. D. Zhu, Z. F. Yue and Z. Z. Wu, Chem. J. Chinese Univ., 12 (1991) 1066.
4 X. G. Cui and D. X. Liu, J. Inorg. Chem., 8 (1992) 329.
5 X. G. Cui and X. Y. Li, Acta Chimica Sinica, 51 (1993) 346.
6 D. X. Liu and X. G. Cui, Chem. J. Chinese Univ., 10 (1989) 787.
7 B. N. Achar, Proc. Int. Clay. Conf., Jerusalem 1966. Vol. 1, p. 67.
8 A. W. Coats and J. P. Redfern, Nature (London), 201 (1964) 68.